

Multivariate Change Detection on High Resolution Monovariate SAR Image Using Linear Time-Frequency Analysis

A. Mian^{*‡}, J.P. Ovarlez^{*†}, G. Ginolhac[‡] and A. Atto[‡]

^{*}SONDRA, CentraleSupelec, FRANCE

Email: ammar.mian@centralesupelec.fr

[†]ONERA, FRANCE

[‡]LISTIC, Université Savoie Mont-Blanc, FRANCE

Abstract—In this paper, we propose a novel methodology for Change Detection between two monovariate complex SAR images. Linear Time-Frequency tools are used in order to recover a spectral and angular diversity of the scatterers present in the scene. This diversity is used in bi-date change detection framework to develop a detector, whose performances are better than the classic detector on monovariate SAR images.

Index Terms—Change Detection, High-resolution SAR, Monovariate Image, Linear Time-Frequency Analysis

I. INTRODUCTION

In Remote Sensing, CD (Change detection) consists in using several images in order to detect or measure the changes occurring in a scene of interest. The information about the changes are important in several practical uses such as land monitoring or quantifying deforestation and urban expansion. The images can be obtained through passive (Optic) or active (Radar) sensors. SAR (Synthetic Aperture Radar) sensors are in peculiar promising for their sensing capabilities in all weather situations and all light conditions. The ground-resolution achieved with recent sensors is interesting as well.

Several methods for CD in SAR images have been investigated in the recent years [1]. For monovariate images, the most simple approach is to derive a GLRT (Generalised Likelihood Ratio Test) by estimating the variance of a pixel (supposed Gaussian) for both images [2]:

$$\hat{\Lambda}_{\text{GLRT-mono}} = \frac{\left(\sum_{k=1}^K |x_k|^2 + \sum_{k=1}^K |y_k|^2 \right)^2}{\sum_{k=1}^K |x_k|^2 \sum_{k=1}^K |y_k|^2} \quad (1)$$

x_k is the value of the pixel in image 1 and y_k in the image 2. The variances are estimated using a window around the pixel corresponding to K samples. This algorithm does not exploit the phase and is often referred as an Incoherent CD technique.

Some SAR systems produce multivariate Images of the scene, meaning that each pixel is represented by a data vector.

PolSAR (Polarimetry SAR) is an example: each element of the data vector corresponds to the backscattering coefficient from the scatterers in the zone of the pixel in a single polarimetric mode (HH, VV or VH). Multivariate images present a greater diversity for each pixel than monovariate ones. In this case, we can expect better performances in CD for multivariate images than monovariate ones. Recent works have been done to extend the monovariate algorithms in the multivariate case [3], [4], [5], [6]. Those works exploit polarimetric diversity to improve the CD results. It can be wondered if apart from Polarimetry, different sources of diversity are profitable in CD. This could prove fruitful in cases where polarimetric diversity is not available. Indeed, PolSAR necessitates sensors with capabilities of emitting the electromagnetic waves in peculiar modes which are not always available. Thus, often the only resources available are complex single look monovariate images of the scene.

The recent advances in technology have improved the resolution on the images. An assumption done in traditional low-resolution SAR image reconstruction is that all scatterers are white and isotropic. We assume that the scatterers present in the scene will respond to an electromagnetic wave in all directions and in all frequencies. This hypothesis is reasonable for low-resolution SAR systems, but it was shown ([7], [8], [9], [10], [11], [12]) that for recent high-resolution SAR imagery, it does no longer apply. The scatterers can have a peculiar signature in angle and frequency domains. We call these, colored scatterers. This spectral and angular non-stationary behaviour of scatterers can be due to their material (dispersive), orientation (anisotropic) or geometry (anisotropic and dispersive). This spectral and angular diversity is interesting in the problematic of CD on monovariate images. However, how can we retrieve this information?

Several tools can be used in order to unphase the angular and spectral diversity. For example, by using geometric image transforms such as steerable pyramids [13], [14], curvelets [15] or sub-space projection [16], [17]. In this paper, we

propose to use a linear Time-Frequency analysis based on the SAR geometry in order to retrieve the information. In [18], the use of 2D wavelet transforms is used to fetch the information about the spectral and angular response of the scatterers present in the scene. The approach is used to detect targets embedded in a clutter.

We propose in this paper to take advantage of this methodology, in the CD framework, in order to perform the multivariate algorithms using spectral and angular diversity.

Section II presents a generalisation of monovariate CD techniques in multivariate case. These techniques will be used with the vectors obtained through the decomposition presented in section III. Section IV provides experimental results obtained through simulation on a SAR Image and Section V concludes the work.

II. CHANGE DETECTION PROBLEM

In this section, we formalise the change detection problem in the multivariate case.

Suppose we have two images \mathbf{I} and \mathbf{J} of size M and have each pixel of size p at two different dates:

$$\begin{cases} \mathbf{I} = [\mathbf{i}_1, \mathbf{i}_2, \dots, \mathbf{i}_M] \in \mathbb{C}^{p \times M} \\ \mathbf{J} = [\mathbf{j}_1, \mathbf{j}_2, \dots, \mathbf{j}_M] \in \mathbb{C}^{p \times M} \end{cases}$$

The Neyman-Pearson detector has been derived by Novak in the Gaussian case [3]. If $\forall k, \mathbf{i}_k \sim \mathcal{CN}(\mathbf{0}_p, \mathbf{C}_i)$ and $\mathbf{j}_k \sim \mathcal{CN}(\mathbf{0}_p, \mathbf{C}_j)$, the change on a pixel is detected through a change in its covariance matrix \mathbf{C} which is estimated on a windows of K samples around the pixel. The detection problem can be written as follows:

$$\begin{cases} H_0 : \mathbf{C}_i = \mathbf{C}_j \\ H_1 : \mathbf{C}_i \neq \mathbf{C}_j \end{cases}$$

Under those assumptions, the GLRT is given by:

$$\hat{\Lambda}_{\text{GLRT-multi}} = \frac{\left| \frac{1}{2K} \left(\sum_{k=1}^K \mathbf{i}_k \mathbf{i}_k^H + \sum_{k=1}^K \mathbf{j}_k \mathbf{j}_k^H \right) \right|^{2K}}{\left| \frac{1}{K} \sum_{k=1}^K \mathbf{i}_k \mathbf{i}_k^H \right|^K \left| \frac{1}{K} \sum_{k=1}^K \mathbf{j}_k \mathbf{j}_k^H \right|^K}. \quad (2)$$

We recognize here, the Sample covariances matrices of the data on \mathbf{I} and \mathbf{J} :

$$\hat{\mathbf{C}}_i = \frac{1}{K} \sum_{k=1}^K \mathbf{i}_k \mathbf{i}_k^H \quad \text{and} \quad \hat{\mathbf{C}}_j = \frac{1}{K} \sum_{k=1}^K \mathbf{j}_k \mathbf{j}_k^H. \quad (3)$$

Those are the Maximum Likelihood Estimators when the data is modelled as Gaussian.

III. CONSTRUCTION OF SPECTRAL AND ANGULAR DIVERSITY

This section presents the methodology adopted to achieve spectral and spatial diversity using solely a complex monovariate image.

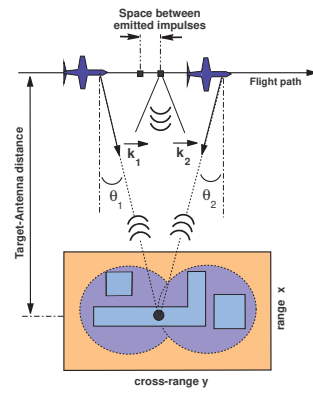


Fig. 1: A reflector, viewed at two different azimuthal angles of illumination in SAR-stripmap mode.

A. SAR Image construction

Synthetic Aperture Radar Imaging is done by emitting an electromagnetic wave through a moving radar and analysing the backscattering signal in order to obtain a map of the scatterers of the scene. The figure 1 presents the principle and the geometry of the acquisition for a stripmap SAR. The radar moves along the axis y called the azimuth which allows it to observe the scene several times at different looking angle θ . The signal emitted is located in a certain range of frequencies and its bandwidth B determines the range resolution of the radar. \mathbf{k} represents the wave vector and it is related to the emitted frequency by $|\mathbf{k}| = k = 2f/c$ (c being the celerity of the light) and the angle of illumination by $\theta = \arg(\mathbf{k})$. Then, $\mathbf{k} = [k_x, k_y]^T = [k \cos(\theta), k \sin(\theta)]^T$.

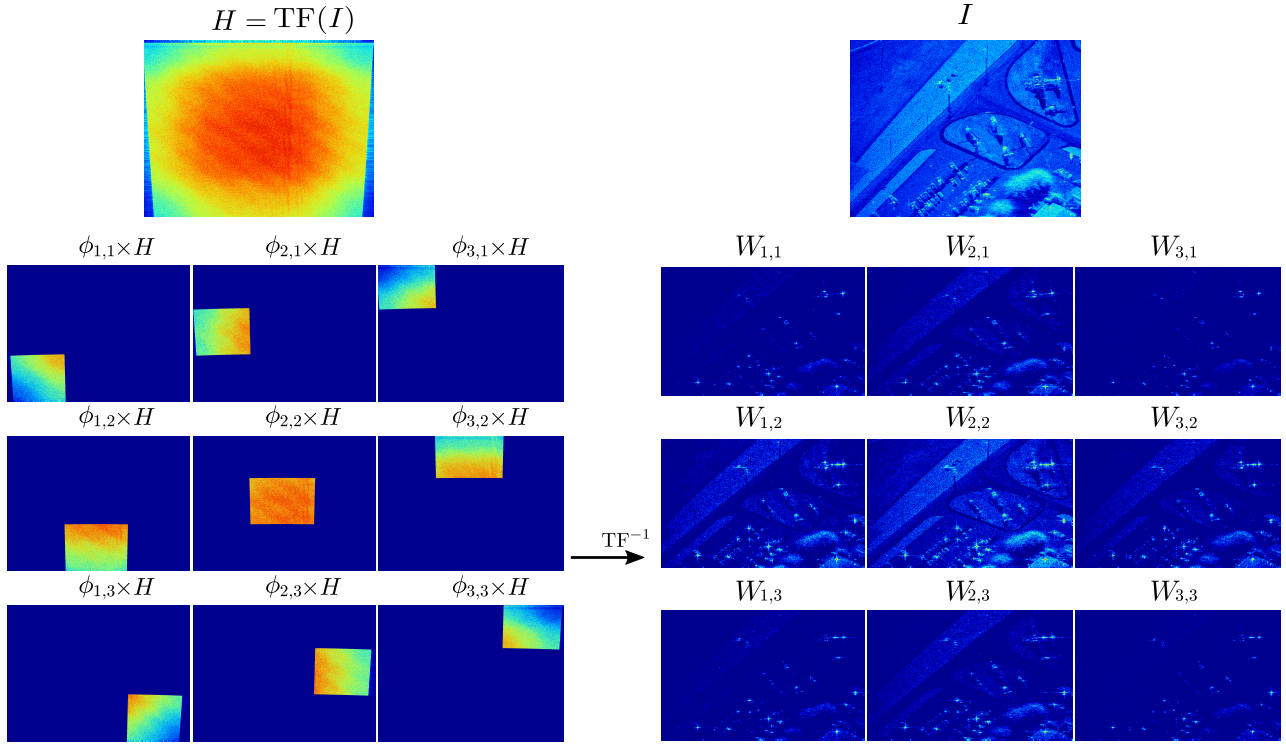
Each scatterer is located at a position $\mathbf{r} = [x, y]^T$ and has a reflection coefficient $I(\mathbf{r})$ that is supposed to be the same for all the frequencies f and looking angle θ . The map of all the reflection coefficient corresponds to the reconstructed image of the scene. In usual SAR reconstruction algorithms (i.e. Range Migration Algorithm [19]), a step is the computation of the Radar Cross Section $H(\mathbf{k})$. Then, a Stolt interpolation is done to go from polar to Cartesian coordinates. Finally, the reconstructed image is obtained by a means of an IFT2 (Inverse Fourier Transform 2D) on k_x and k_y :

$$I(\mathbf{r}) = \iint_{\mathbb{R}^2} H(k_x, k_y) e^{2j\pi(k_x x + k_y y)} dk_x dk_y \quad (4)$$

B. Linear Time-Frequency analysis of SAR Images

When colored scatterers are present in the scene imaged, the IFT2 results in a loss of information about the specificities of their response. In [18], it is proposed to use 2D wavelet transform in order to create several sub-images corresponding to a certain range of frequencies and angles.

In this paper, we propose to simplify the method and use a Short Time Fourier Transform. Suppose, we have an image whose spectrum has the definition domain $\Delta = [k_{\min}, k_{\max}] \cup [\theta_{\min}, \theta_{\max}]$. The range of frequencies available is of size $\kappa =$

Fig. 2: Example of decomposition with $N_k, N_\theta = 3, 3$

$k_{\max} - k_{\min}$ and the range of angles is of size $\Theta = \theta_{\max} - \theta_{\min}$. We can define the function $\phi_{l,m}(k, \theta)$:

$$\phi_{l,m}(k, \theta) = \begin{cases} 1 & \text{if } (k, \theta) \in \Delta_{l,m} \\ 0 & \text{otherwise} \end{cases} \quad (5)$$

with

$$\begin{aligned} \Delta_{l,m} = & \left[k_{\min} + \frac{(l-1)\kappa}{N_k}, k_{\min} + \frac{l\kappa}{N_k} \right] \\ & \cup \left[\theta_{\min} + \frac{(m-1)\Theta}{N_\theta}, \theta_{\min} + \frac{m\Theta}{N_\theta} \right]. \end{aligned} \quad (6)$$

$\phi_{l,m}$ is a moving window on H to select a range of angles and frequencies. The size of the window determines the number of sub-bands N_k and sub-angles N_θ . A sub-image can be computed by means of an IFT2 on $\phi_{l,m} \times H$:

$$W_{l,m}(\mathbf{r}) = \int_0^{2\pi} d\theta \int_0^{+\infty} k H(k, \theta) \phi_{l,m}(k, \theta) e^{+j2\pi\mathbf{k}^T \mathbf{r}} dk \quad (7)$$

The figure 2 shows an example of decomposition for a SAR image. We can interpret it as a multivariate image. Indeed, for each pixel, we can associate a $p = N_k \times N_\theta$ vector of data \mathbf{i} corresponding to the value of the pixel in each of the $W_{l,m}$ images: $\mathbf{i} = [W_{1,1}(x, y), W_{1,2}(x, y), \dots, W_{N_k, N_\theta}(x, y)]^T$.

In practice, the image obtained must be decimated according to the incertitude principle: the support of the window being more limited in angular and frequency than

the whole image, its spatial power of resolution is impacted. Consequently the image is decimated by a factor N_θ in the azimuth direction and N_k in the range direction.

This approach allows to retrieve a diversity that was lost during the construction of the single look monovariate image. It is relevant in our problem of change detection as it constitute a diversity that can be exploited in the algorithms presented in the introduction. We can assume that a change in the scene implies that the angular and spectral behaviour of the reflectors varies as well. This allows in theory a more precise detection of a change than working on the amplitude alone.

IV. SIMULATIONS

This section describes simulations done on monovariate SAR images. It presents the results obtained using the decomposition presented in section III and compares then to the classic monovariate algorithm.

A. DataSet

Figure 3 shows a SAR Image of static aircraft available from Sandia National Laboratories (http://www.sandia.gov/radar/complex_data/). This image was used in the following simulations. For all simulations presented here, we chose $N_k = 5$ and $N_\theta = 5$. Having only a single image, a change is to be simulated on the image in order to compute the change detection algorithms. For simplicity's sake, only punctual targets are added on the

image at random positions.

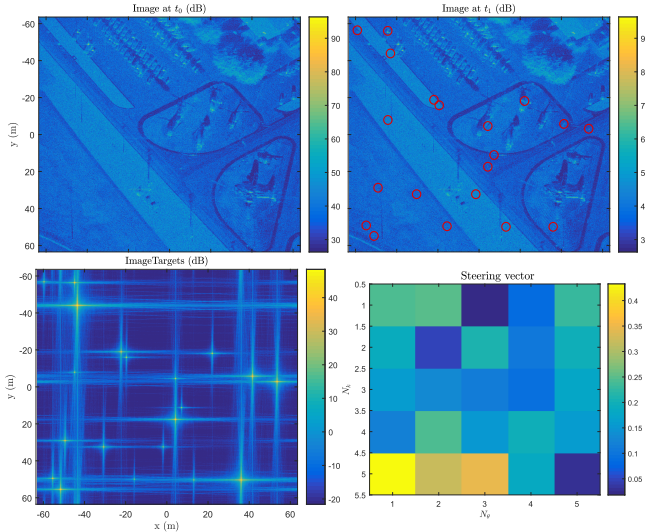


Fig. 3: Example of change generated (SNR: random between $[0; 30]$ dB, position: random on the image). Top-Left: Image I. Top-Right: Image J (changes are circled in red). Bottom-Left: Image of targets. Bottom-Right: Steering vector of one target.

The steering vector is chosen through a random complex Gaussian distribution. The SNR of the targets can be controlled by choosing the norm of the steering vector. It enables us to measure statistical performances. The SNR is defined as the ratio of the target power and the mean power value of a square window of size 20×20 around the position of the target. Additional Gaussian noise was added into the image to take into account the difference in speckle, and its variance was estimated on the dark zones of the image.

The figure 3 shows an example of image with 20 targets of random SNR between 0 and 30 dB.

B. Results

Figure 4 shows the plots of P_{FA} -threshold for both monovariate and multivariate algorithms. These were computed using the detection algorithms between the image at t_0 and an image t_1 generated without change. The curves were plotted for several sizes of analysis windows. We can see that its size is an important parameter in the multivariate case: for the multivariate GLRT, a size of 5×5 the P_{FA} is not well regulated as the number of secondary data for the estimation of the covariances matrices is the bare minimum. Having a large window allows a better regulation, but a too large window affects the performances of detection.

We choose to test the detection performances with a window of 7×7 for $\hat{\Lambda}_{GLRT\text{-multi}}$ and 5×5 for $\hat{\Lambda}_{GLRT\text{-mono}}$ and for a P_{FA} fixed for 10^{-3} . The threshold for the detection is obtained using the curves at Figure 4. Figure 5 shows the detection test for both algorithms on the example presented at Figure 3. We notice that in the multivariate case, the detector performs better. Indeed, some low SNR targets, which

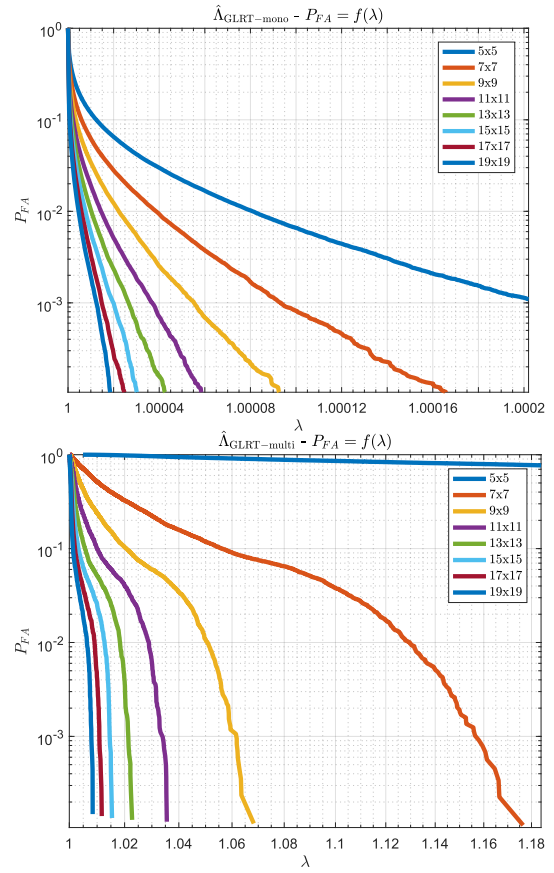


Fig. 4: $P_{FA} = f(\lambda)$ for different sizes of window (computed on 1500×1500 samples). Top : $\hat{\Lambda}_{GLRT\text{-mono}}$. Bottom: $\hat{\Lambda}_{GLRT\text{-multi}}$.

were not detected in monovariate case, are detected using the multivariate algorithm (circled in red). There is also less false alarms on the test image. We note that the localisation of the detection is degraded because of the decimation. There is a compromise to be done between the precision we want and the expected performances of detection. This is done by choosing the number of sub-bands and sub-looks.

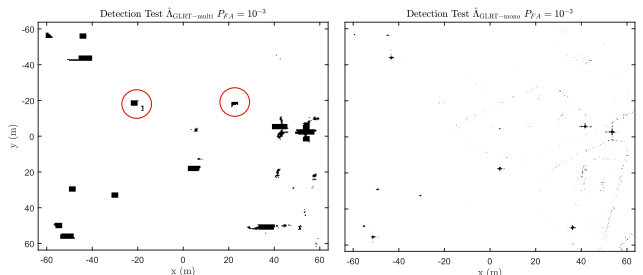


Fig. 5: Detection test at $P_{FA} = 10^{-3}$. Left: $\hat{\Lambda}_{GLRT\text{-multi}}$ (7×7). Right: $\hat{\Lambda}_{GLRT\text{-mono}}$ (5×5).

Monte-Carlo trials have been done in order to measure the statistical performances of the new detector and compare it to the monovariate one. A single target is placed at a random location which varies for each trial. Figure 6 shows a ROC (Radar Operational Curve) plot for a SNR defined at -5 dB.

We can see that the multivariate detector performs better, especially at low P_{FA} where the P_D is better by at least 0.2.

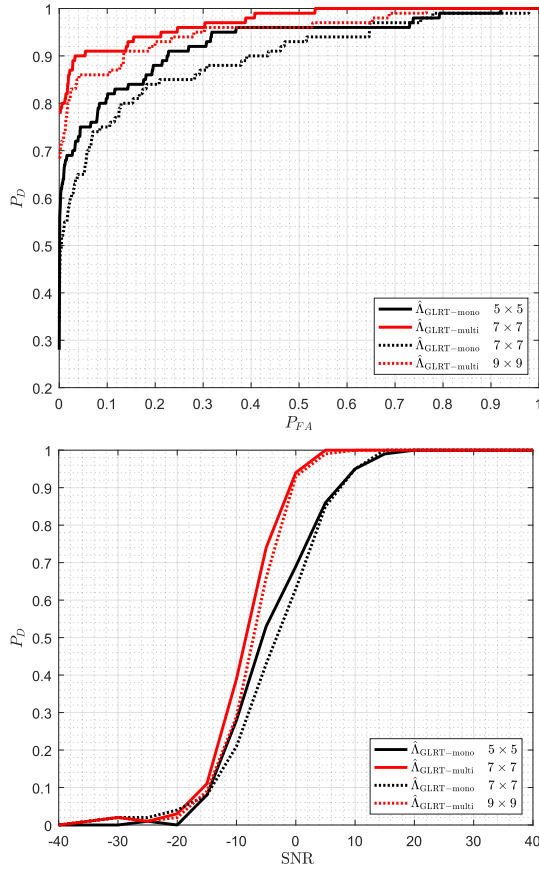


Fig. 6: Top: $P_D = f(P_{FA})$ computed on 100 Monte-Carlo trials (SNR = -5 dB, random position of the target and random steering vector). Bottom: $P_D = f(\text{SNR})$ computed on 100 Monte-Carlo trials ($P_{FA} = 10^{-3}$, random position of the target and random steering vector).

Figure 6 shows a P_D -SNR plot for $P_{FA} = 10^{-3}$. The probability of detection is similar at low SNR, which is expected as the target is shrouded in the clutter. For the range of SNR $[-15, 20]$ dB, the performances of the multivariate detector are better. Indeed, for a given P_D , a SNR gain is noticed: at least 1 dB for $P_D = 0.2$ and as much as 10 dB for $P_D = 0.9$. These simulations show that the multivariate GLRT performs better overall than the monovariate GLRT.

V. CONCLUSION

This paper proposed a new methodology for CD on monovariate SAR images and tested it through simulations which demonstrated better performances than the classic algorithm on monovariate images. The increased performances are obtained with a compromise on the spatial resolution of the detection. Nonetheless, the spectral and angular diversity allows for a more accurate detection of the change in terms of probability of detection.

This work was done using a Gaussian model for the data, which is a questionable hypothesis for highly-textured images. It will be extended to SIRV and CES distributions in future works.

REFERENCES

- [1] M. Hussain, D. Chen, A. Cheng, H. Wei, and D. Stanley, "Change detection from remotely sensed images: From pixel-based to object-based approaches," *ISPRS Journal of Photogrammetry and Remote Sensing*, vol. 80, pp. 91 – 106, 2013. [Online]. Available: <http://www.sciencedirect.com/science/article/pii/S0924271613000804>
- [2] Y. Hsu, H.-H. Nagel, and G. Rekers, "New likelihood test methods for change detection in image sequences," *Computer Vision, Graphics, and Image Processing*, vol. 26, no. 1, pp. 73 – 106, 1984. [Online]. Available: <http://www.sciencedirect.com/science/article/pii/0734189X84901312>
- [3] L. M. Novak, "Change detection for multi-polarization multi-pass sar," in *Defense and Security*. International Society for Optics and Photonics, 2005, pp. 234–246.
- [4] ———, "Coherent change detection for multi-polarization sar," in *Conference Record of the Thirty-Ninth Asilomar Conference on Signals, Systems and Computers*, 2005., Oct 2005, pp. 568–573.
- [5] M. Preiss and N. J. S. Stacy, "Polarimetric sar coherent change detection," in *7th European Conference on Synthetic Aperture Radar*, June 2008, pp. 1–4.
- [6] J. Barber, "A generalized likelihood ratio test for coherent change detection in polarimetric sar," *IEEE Geoscience and Remote Sensing Letters*, vol. 12, no. 9, pp. 1873–1877, Sept 2015.
- [7] J. Bertrand and P. Bertrand, "The concept of hyperimage in wide-band radar imaging," *Geoscience and Remote Sensing, IEEE Transactions on*, vol. 34, no. 5, pp. 1144–1150, Sep. 1996.
- [8] J. P. Ovarlez, L. Vignaud, J. C. Castelli, M. Tria, and M. Benidir, "Analysis of sar images by multidimensional wavelet transform," *IEE Proceedings - Radar, Sonar and Navigation*, vol. 150, no. 4, pp. 234–241, Aug. 2003.
- [9] M. Tria, J. P. Ovarlez, L. Vignaud, J. C. Castelli, and M. Benidir, "Discriminating real objects in radar imaging by exploiting the squared modulus of the continuous wavelet transform," *IET Radar, Sonar and Navigation*, vol. 1, no. 1, pp. 27–37, Feb. 2007.
- [10] M. Duquenoy, J. P. Ovarlez, L. Ferro-Famil, E. Pottier, and L. Vignaud, "Scatterers characterisation in radar imaging using joint time-frequency analysis and polarimetric coherent decompositions," *IET Radar, Sonar and Navigation*, vol. 4, no. 3, pp. 384–402, June 2010.
- [11] F. Brigui, L. Thirion-Lefevre, G. Ginolhac, and P. Forster, "New sar algorithm based on orthogonal projections for mmst detection and interference reduction," *IEEE Transactions on Geoscience and Remote Sensing*, vol. 52, no. 7, pp. 3800–3811, July 2014.
- [12] F. Brigui, G. Ginolhac, L. Thirion-Lefevre, and P. Forster, "New sar target imaging algorithm based on oblique projection for clutter reduction," *IEEE Transactions on Aerospace and Electronic Systems*, vol. 50, no. 2, pp. 1118–1137, April 2014.
- [13] E. P. Simoncelli, W. T. Freeman, E. H. Adelson, and D. J. Heeger, "Shiftlet multiscale transforms," *Information Theory, IEEE Transactions on*, vol. 38, no. 2, pp. 587–607, March 1992.
- [14] M. Unser, N. Chenouard, and D. V. D. Ville, "Steerable pyramids and tight wavelet frames in," *Image Processing, IEEE Transactions on*, vol. 20, no. 10, pp. 2705–2721, Oct 2011.
- [15] E. Candès, L. Demanet, D. Donoho, and L. Ying, "Fast discrete curvelet transforms," *Multiscale Modeling & Simulation*, vol. 5, no. 3, pp. 861–899, 2006. [Online]. Available: <http://dx.doi.org/10.1137/05064182X>
- [16] G. Ginolhac, L. Thirion-Lefevre, R. Durand, and P. Forster, "Sar processors based on signal or interference subspace detector," *IEEE Transactions on Aerospace and Electronic Systems*, vol. 46, no. 3, pp. 1006–1020, July 2010.
- [17] R. Durand, G. Ginolhac, L. Thirion, and P. Forster, "New sar processor based on matched subspace detectors," *IEEE Transactions on Aerospace and Electronic Systems*, vol. 45, no. 1, pp. 221–236, Jan 2009.
- [18] J.-P. Ovarlez, G. Ginolhac, and A. M. Atto, "Multivariate linear time-frequency modeling and adaptive robust target detection in highly textured monovariate sar image," *International Conference on Acoustics, Speech, and Signal Processing*, 2017, p. to appear.
- [19] M. Soumekh, *Synthetic Aperture Radar Signal Processing with MATLAB Algorithms*. New York: John Wiley and Sons, 1999.